Hygroscopic Growth of Multicomponent Aerosol Particles Influenced by Several Cycles of Relative Humidity

Thomas Rosenoern, Julie C. Schlenker, and Scot T. Martin*

School of Engineering and Applied Sciences & Department of Earth and Planetary Sciences, Harvard University, Cambridge, Massachusetts 02138

Received: September 6, 2007; In Final Form: November 27, 2007

Infrared aerosol flow tube experiments were performed for mixtures of ammonium, sulfate, and hydrogen ions at 293 K. The impact of the cycling of relative humidity (RH) on the crystals formed and on the hygroscopic growth was evaluated. Submicron particles having an extent of neutralization (X) between 0.60 and 0.75 were the focus, with special emphasis on the composition of aqueous letovicite $(NH_4)_3H(SO_4)_2$ ($X = 0.75$) because of its unique behavior. Aqueous letovicite particles crystallized initially as an external mixture of solid particles, forming pure particles of letovicite $(NH_4)_3H(SO_4)_2$(s) (LET) in some cases and internally mixed particles of ammonium sulfate ($(NH_4)_2SO_4$(s);AS) and ammonium bisulfate (NH_4HSO_4(s); AHS) in other cases. Cycling between 3% and 48% RH increased the fraction of LET particles in the aerosol population, moving in the direction of the more thermodynamically favored species. However, some internally mixed particles remained even after multiple cycles, possibly indicative of a memory effect of AS as a heterogeneous nucleus for AHS. For all compositions studied, the RH of first water uptake and the magnitude of water uptake at higher RH were compared to model predictions. As expected, the more acidic particles ($X = 0.60$ and 0.65) took up water at the eutonic RH (37%) of mixed AHS/LET particles, but not as expected, both solids dissolved completely, arguing for an increased water solubility possibly attributable to nanocrystalline materials. Particles of $X = 0.70$ took up water above 41% RH, suggesting a particle morphology of an outer coating of AHS that prevents water uptake at the lower eutonic RH values of mixed AHS/LET and AHS/AS particles. Particles of $X = 0.75$ took up water as expected for an externally mixed particle population of LET and AS/AHS particles, although the fraction of each type in the population depended on the RH history. These results show that the hysteresis effect for some particles depends on a multi-node RH history. The implication for atmospheric particles is that the crystals present therein as well as particle morphology, water content, and extent of internal/external mixing might continue to evolve during multiple atmospheric cycles of RH.

1. Introduction

Atmospheric particles influence the Earth's radiation balance and therefore climate by scattering and absorbing incoming solar radiation.[1] The effects depend on the interactions of the particles with atmospheric water vapor. Sulfate on a global basis constitutes the largest anthropogenic contribution to the mass budget of atmospheric particles and contributes a significant cooling term to the Earth's energy balance.[2] The magnitude of the cooling depends directly on the physical state of the particles,[3] namely whether they are aqueous or solid,[4] because the particle light scattering efficiency varies with state-dependent properties such as diameter and refractive index.[5] Sulfate particles also influence the chemistry of the atmosphere by providing surfaces for heterogeneous reactions and serving as sinks and sources of atmospheric gases,[6,7] and the reaction rates can depend on the physical state of the particles. For example, N_2O_5 hydrolysis, a key reaction in controlling tropospheric OH and NO_x concentrations, is 10^3 times faster on aqueous than solid particles.[8] Accurate predictions of the effects of sulfate particles on radiative forcing and atmospheric chemistry therefore require knowledge of the particle physical state.

The phase-transition behavior of sulfate particles depends on the chemical composition. In our previous work, focusing on sulfate−nitrate−ammonium (SNA) particles,[9] we observed that for certain chemical compositions aqueous particles crystallized as metastable solids at low relative humidity, in agreement with Ostwald's rule of stages. The metastable solids then recrystallized to more thermodynamically stable crystals at higher relative humidity.[10,11] The recrystallization was facilitated by an increase in ion mobility caused by adsorbed water. Furthermore, we found that some SNA particles retained liquid water as enclosed pockets at relative humidities below the efflorescence point, even though the particle diameters were smaller than 500 nm,[12] in analogy to a similar report for NaCl particles from Weis and Ewing.[13] Enclosed water pockets were also observed by Colberg et al.[14] for 2−20 μm particles. Organic molecules[15−23] and insoluble minerals[24−26] mixed with SNA particles further influence phase transitions and particle morphology.

For the experiments reported herein, we systematically investigate the dependence of the presence of metastable phases and liquid water on the cycling of relative humidity. On the basis of our earlier preliminary observations of compositions having complex crystallization behavior,[9,12] we focus on the aqueous chemical composition corresponding to letovicite (i.e., 3 parts NH_4^+, 1 part H^+, and 2 parts SO_4^{2-}). The particles are subjected to repeated cycles of low and medium RH, maintain-

* Corresponding author. E-mail: scot_martin@harvard.edu. http://www.seas.harvard.edu/environmental-chemistry.

10.1021/jp0771825 CCC: $40.75
Published on Web 02/26/2008

ing the condition that RH does not exceed the RH of complete deliquescence. We also make comparisons of the results obtained for the letovicite composition to those obtained for more acidic particles. In our earlier work,[12] we found no residual water for particles more neutralized than letovicite so no further experimental work is conducted herein for those compositions.

2. Experimental Approach

2.1. Chemical Compositions Studied. The chemical compositions of SNA particles can be described in a two-dimensional $X-Y$ coordinate space.[9,12] X is the fraction of cations due to ammonium, with the balance coming from proton (i.e., the degree of neutralization), and Y is the fraction of anions due to sulfate with the balance coming from nitrate:

$$X = \text{moles of } NH_4^+/(\text{moles of } NH_4^+ + \text{moles of } H^+) \quad (1a)$$

$$Y = \text{moles of } SO_4^{2-}/(\text{moles of } SO_4^{2-} + \text{moles of } NO_3^-) \quad (1b)$$

The compositions used in the current study, all of which are along the $Y = 1$ axis, are denoted as [X, 1]. Particles of $Y = 1$ have varying amounts of $(NH_4)_2SO_4$ and H_2SO_4 and no nitrate. The [X, Y] notation is used so that comparisons with our previous work can be made easily. For the X value, we focus mostly on observations for the composition having $X = 0.75$ (corresponding to letovicite) and make comparisons for results obtained for $0.60 \leq X < 0.75$. Solid phases of [X, 1] include ammonium bisulfate (AHS, [0.5, 1], NH_4HSO_4), letovicite (LET, [0.75, 1], $(NH_4)_3H(SO_4)_2$), and ammonium sulfate (AS, [1,1], $(NH_4)_2SO_4$). Further orientation on the phase diagrams and phase transitions of this system is available from many sources (e.g., refs 4, 12, and 14).

2.2. AFT-IR Experiments. The experimental apparatus was described previously.[9] Aqueous particles in nitrogen gas were produced with a TSI 3076 atomizer from 1 M reservoir solutions of composition [X, 1]. Following atomization, the aqueous droplets were equilibrated to 66% RH to ensure that all particles had the same water activity at the beginning of the experiment. The particles remained aqueous because the crystallization relative humidities of compositions [X, 1] lie between 0 and 35% RH.[9] The aerosol flowed at 3 Lpm through a series of cells containing sulfuric acid solutions of different concentrations that adjusted the aerosol relative humidity to desired values. The cells were kept at 293 K, and the volume-equivalent residence time was 210 s.[9] For each of the compositions [0.60, 1], [0.65, 1], [0.70, 1], and [0.75, 1], the following five relative humidity histories were applied, and the infrared observations from each were analyzed and compared: (1) 66 → *xx*, (2) 66 → 3 → *xx*, (3) 66 → 3 → *yy* → 3, (4) 66 → 3 → *yy* → 3 → *xx*, and (5) 66 → 3 → *yy* → 3 → *yy* → 3 → *xx*, where *xx* and *yy* can be similar or different values of RH. Care was taken that *xx* and *yy* were maintained below the relative humidity of complete deliquescence predicted by the Aerosol Inorganics Model[27] for the mixed particles assuming that the thermodynamically most stable solids crystallized at 3% RH (i.e., corresponding to the intersections of curves 1 and 8 in Figure 5).

The presence of solids for each RH history and their composition were determined by infrared spectroscopy. There were characteristic peak positions between 600 and 1500 cm^{-1} for each of AHS, LET, and AS.[12] Extinction spectra were recorded (400 scans, 1 cm^{-1} resolution) as the RH-processed aerosol flowed through a 90 cm detection cell. Extinction resulted both from the absorbance of gases and particles and from the scattering by particles. Reference gas-phase water spectra were collected before and after each experiment by exposing a particle-free N_2-flow to the same RH program as the aerosol. These gas-phase water absorbance spectra were subtracted from the aerosol extinction spectra, leaving residual spectra corresponding to the particles. These residual spectra are shown in all figures of this paper.

2.3. Peak Area Measurements. The relative liquid water content of the particles was determined by integrating the area of the O−H stretch that occurs at approximately 3450 cm^{-1}. The spectra were normalized to the N−H stretch at 3300 cm^{-1} to account for any differences in particle loading. After the baseline was fit from 1900 to 3600 cm^{-1} to account for scattering, the O−H and N−H stretches were fit simultaneously with Gaussian peaks:

$$E(\tilde{\nu}) = Ae^{-[(\tilde{\nu} - (\tilde{\nu}_0))/\Gamma]^2} \quad (2)$$

where E is the extinction, A is the peak amplitude, $\tilde{\nu}$ is the wavenumber, $\tilde{\nu}_0$ is the peak center, and Γ is the peak width at half-maximum. Compared to Lorentz or Voigt peaks, the Gaussian shape gave the best fit to the observed spectra. The peak area of the O−H stretch was determined by integrating $E(\tilde{\nu})$ using the determined values of A, $\tilde{\nu}_0$, and Γ. The peak area was assumed as proportional to the liquid water content, although there may have been some minor nonlinearity because of changes in the optical constants with water activity and chemical composition as well as changes in the size distribution with hygroscopic growth. The uncertainty of the liquid water content based on the fitting procedure is approximately 10% of the fitted value, corresponding to an uncertainty in the peak area ratios of 0.1.

3. Results and Discussion

Figure 1 shows the effect of repeated RH cycling on the infrared spectrum of particles having composition [0.75, 1]. In regard to liquid water, for our purposes we focus on the spectral band around 3450 cm^{-1}. For solid phases, we focus on the spectral features below 1600 cm^{-1}. After exposure to 66 → 56%, corresponding to RH program #1, the particles do not crystallize,[14,28−30] as indicated by the large absorption of liquid water. The particles are solution droplets on the upper side of the hysteresis loop. For RH program #2, prior to 56% RH the particles are exposed to 3% RH, possibly allowing the formation of AS, AHS, or LET, all of which are supersatured for [0.75, 1] at 3% RH. The thermodynamic prediction is that letovicite should form and no liquid water should remain. Moreover, there should be no dissolved solid mass until the deliquescence of letovicite at 69% RH.[28] The difference in water content for RH program #2 compared to #1 demonstrates that crystallization at least partially occurs, as expected for 3% RH. However, the spectrum of RH program #2 shows that liquid water remains. Regarding the nature of this water, the spectrum corresponding to 66 → 3 → 48% shows that less water is present compared to 66 → 3 → 56% RH, indicating that the water is not tightly locked within the particle structure but rather is in equilibrium with the gas phase. A fraction of the liquid water evaporates as water activity decreases.

The spectra at 56% RH in the top panel of Figure 1 show that exposing the particles again to 3% RH before restoring to 56% RH (i.e., a second cycle of drying; RH program #4) reduces the liquid water content. This decrease indicates that the undissolved solid mass increases after each RH cycle. A third cycle (i.e., RH program #5) does not significantly further reduce

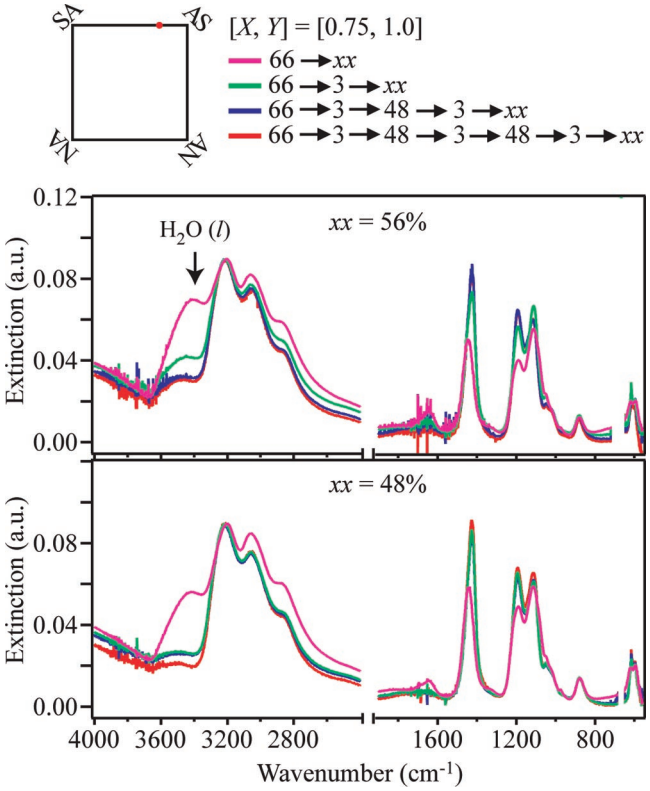

Figure 1. Infrared spectra recorded for RH histories #1, #2, #4, and #5 for *yy* = 48% and (top) *xx* = 56% or (bottom) *xx* = 48% for the composition [0.75, 1]. RH histories are described further in section 2.2. The spectra show that the particle liquid water content decreases as the number of relative humidity cycles increases.

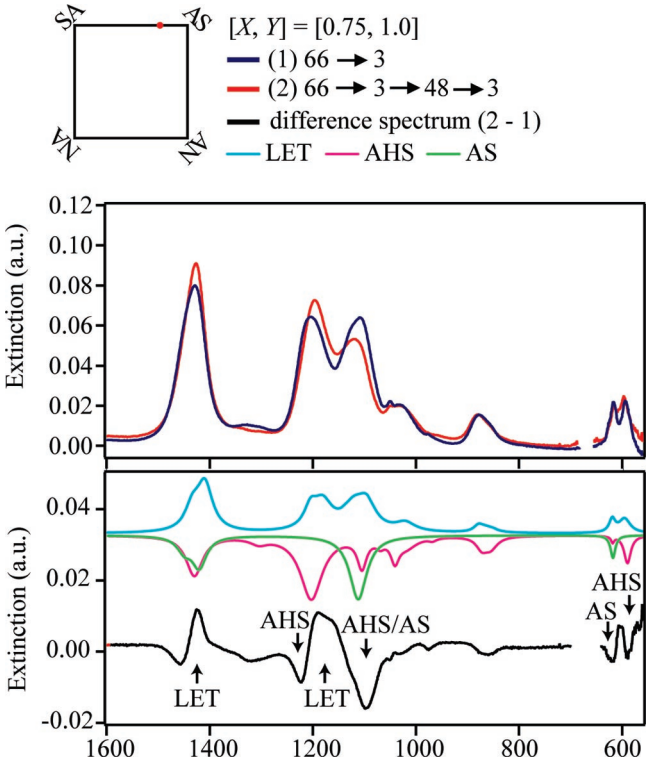

Figure 2. (Top) Effect of an RH cycle on the infrared spectrum of the composition [0.75, 1]. (Bottom) Difference spectrum shows the growth of letovicite and the loss of ammonium sulfate and ammonium bisulfate. Reference spectra of each of these solids are also shown.

the water content. The spectra at 48% RH are shown in the bottom panel of Figure 1. For 48% RH, within experimental uncertainty the water content no longer changes after the second cycle, although there is still more water at 56% than 48% RH for one, two, and three cycles. The explanation for the absence of apparent changes at 48% RH compared to 56% RH could be that lower growth factors at 48% RH do not allow enough water to be taken up for our experimental setup to detect it at a significant level. Another contributing factor could be that there are enclosed water pockets within the particles, hindering the interactions of the aqueous solution with the water vapor in the gas phase. This factor could be more significant at lower RH and could depend on the residence time used in the experiments.

Accompanying the changes in the hygroscopic properties are related changes in the solids present. The top panel of Figure 2 shows infrared spectra (1) after exposure to RH program #1 (66 → 3) and (2) after exposure to RH program #4 (66 → 3 → 48 → 3). The bottom panel shows the difference spectrum of (1) from (2). Reference spectra of LET, AHS, and AS are also shown. LET is shown as a positive spectrum, and the spectra of AHS and AS are inverted for easy comparison with the difference spectrum. The difference spectrum shows that the particle population contains more LET and less AHS and AS upon RH cycling.

The infrared spectra illustrating water uptake for increasingly acidic compositions of [0.75, 1], [0.70, 1], [0.65, 1], and [0.60, 1] are shown in Figure 3. Spectra are shown for RH histories of 66 → 3 → *xx* (i.e., RH program #2), with the final RH varying from 15 to 60%. After the compositions [0.75, 1], [0.70, 1], and [0.65, 1] are exposed to 3% RH, water uptake is not observed until a follow-on RH of 35% or greater. For [0.60, 1], water uptake is not observed until a follow-on RH of 29%. Spectra marked by "∗" for [0.70, 1], [0.65, 1], and [0.60, 1] indicate that the spectra for 66 → 3 → *xx* are identical to those observed for 66 → *xx* (spectra not shown). The water uptake for those RH programs and compositions is thus reversible, indicating the complete deliquescence by an RH of *xx* of solids crystallized at 3% RH. This reversibility begins by 41% RH for [0.60, 1] and 45% RH for [0.65, 1] and [0.70, 1]. In this regard, the composition [0.75, 1] stands out from the others by the absence of reversible water content until at least 60% RH, which is the highest RH value studied in RH program #2. Moreover, in further contrast to [0.75, 1], the spectra corresponding to the other compositions do not have significant changes in peak ratios or locations until water uptake is observed. For those compositions, after water uptake but not prior the ratio of the intensity of the bisulfate peak at 1190 cm^{-1} to that of the sulfate peak at 1120 cm^{-1} smoothly decreases as water content increases, consistent with the chemical equilibrium favoring a shift to sulfate ions with increasing water content. In contrast, for particles of [0.75, 1], the intensity ratio of the bisulfate/sulfate peaks significantly changes from 20 to 35% prior to significant water uptake. The spectral changes, though not shown in detail in the figure, are consistent with shifts from AS/AHS to LET similar to as shown in Figure 2, rather than hydration of aqueous HSO_4^- to form SO_4^{2-}.

A cartoon of the proposed transformations that take place during RH cycles between 3% and 48% is shown in Figure 4 for particles of composition [0.75, 1]. An initial population of aqueous particles crystallizes at 3% RH to form an externally mixed population of solid particles. Although each particle in the aerosol has a stoichiometric composition of [0.75, 1], there is variability in the crystals present among the particles. For some particles, thermodynamically stable letovicite forms. For other particles, internally mixed compositions of ammonium

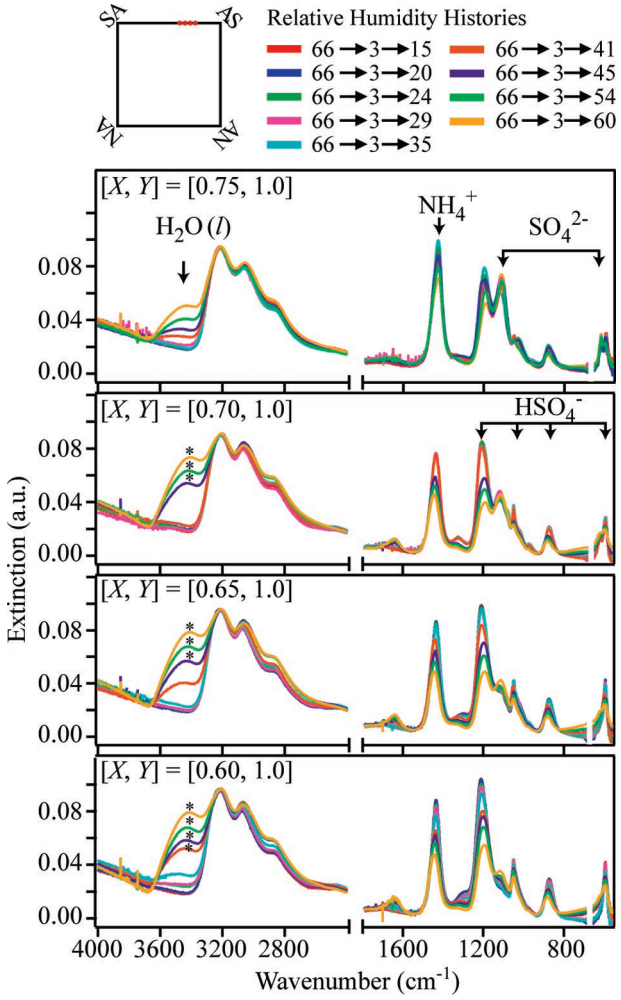

Figure 3. Infrared spectra showing the water uptake for increasingly acidic compositions spanning [0.60, 1] to [0.75, 1]. Spectra are shown for RH histories of 60 → 3 → *xx*, and the final RH varies from 15 to 60%. Spectra marked by "∗" indicate that the shown spectra for 60 → 3 → *xx* are identical to those recorded for 60 → *xx* (spectra not shown). There is thus no hysteresis effect in the water content for those spectra. All spectra are normalized to the NH_4^+ peak at 3215 cm^{-1}.

bisulfate with ammonium sulfate form in a 1:1 ratio. Features unique to each of these solids are apparent in the difference spectrum of Figure 2. When the RH increases to 48%, the LET particles remain solid and unchanged because they do not deliquesce until 69% RH. According to the Aerosol Inorganics Model (AIM),[27] however, the mixed AHS/AS particles take up water beginning at 27% RH by the dissolution of AHS, thereby resulting in particles at 48% RH that contain a partially dissolved AS core (comprising 34% of the sulfate mass in the particle) and an acidic aqueous outer layer of $X = 0.62$ that is saturated with respect to AS. Complete deliquescence of these particles is not anticipated until 72% RH, according to AIM. When the RH drops to 3% in the next cycle, the aqueous solution surrounding the AS core nucleates LET rather than AHS for a fraction of the particles, leading to the dissolution of AS and the full transformation to the thermodynamically more stable LET phase for those particles. As a result, the fraction of LET particles increases, the fraction of AHS/AS particles decreases, and the corresponding water content at 48% RH also decreases. These effects are apparent in the observations of Figures 1 and 2.

The observations, even after repeated RH cycling, of labile water (Figure 1) and the presence of AHS/AS crystals in the infrared spectrum (not shown) can be rationalized by aspects of heterogeneous nucleation.[24,25,31] The key hypothesis of our interpretation is that the active sites[32,33] on the surface of some of the AS cores adapt with repeated RH cycling to AHS and subsequently retain a memory effect.[31,34] Prior to RH cycling, there is an initial population of particles and a distribution of active sites. RH cycling has two effects: a reduction of the AS population by transforming some particles into LET and an adaptation of the actives sites of the remaining population to a memory effect for AHS. According to AIM, the LET saturation ratio at 48% RH is 6.2. At 27% RH, when AHS attains unity saturation, the LET saturation ratio is 14.4. The limit of homogeneous nucleation is uncertain but is greater than 30 according to AIM for a comparison system of aqueous ammonium sulfate at 35% RH.[30] The memory effect might be reduced if the AS cores were held at 48% longer than the RH-cell residence time of 210 s because dynamic reconstruction of the surface might eliminate active sites, although this experiment was not conducted.

Further interpretation of some of the spectral observations in Figures 1−3 is aided by comparison to predictions of the Aerosol Inorganics Model for internally mixed particles.[27] The legend in Figure 5 shows the eight allowed AIM scenarios for the permutation set of the three allowed solids, namely AS, AHS, and LET. In the legend, "Y" indicates that a solid is allowed to form in the model run and "N" indicates that a solid is not allowed to form. The left-hand axis corresponds to the square markers and shows the experimental observed relative water content (based on the integration of the water peak at 3450 cm^{-1}) after exposure to RH histories of 66 → 3 → *xx* (blue points) or 66 → *xx* (red points). The black markers show the effect of repeated RH cycling on water content for particles with composition [0.75, 1]. The right-hand axis corresponds to the lines and shows the relative amounts of liquid water predicted by AIM for each scenario. The RH history of 66 → *xx* corresponds to fully aqueous particles on the upper side of the hysteresis loop (i.e., case 8 of the AIM model). The left-hand axis is scaled to the right-hand axis to give the best agreement between the red points (i.e., aqueous particles) and case 8 of the AIM model.

Predictions of the model runs compared to the experimental observations of the liquid water content are helpful for understanding the solids formed for the different compositions and RH programs. The compositions [0.60, 1] and [0.65, 1] respond as case 2 of the AIM model, suggesting that these particles are composed predominantly of AHS/LET. The infrared spectra (not shown in detail) indicate the absence of AS and the presence of AHS/LET. The abrupt uptake of water between 35 and 41% is consistent with the AIM prediction of the eutonic RH of AHS/LET, corresponding to the RH at which (solid #1 + solid #2 + vapor) transforms to (aqueous solution + less of solid #1 + vapor). To verify the AIM predictions of the eutonic RH values, we also conducted a series of experiments with bulk crystals of AHS, LET, and AS and observed initial water uptake of AHS/LET (37%), AHS/AS (27%), LET/AS (67%), AHS (37%), LET (70%), and AS (80%). An unexpected result, first mentioned for Figure 3 for the spectra marked by "∗" and apparent in Figure 5 by the overlap of the red and blue points above the eutonic RH, is that the hysteresis effect is absent just above the eutonic RH, represented in Figure 5 by a shift from case 2 to case 8. A possible explanation is that the residual crystals are small enough for a nanosize effect on solubility, thus leading to full dissolution above the eutonic RH. Individual particles of 200−300 nm, as in our study, would

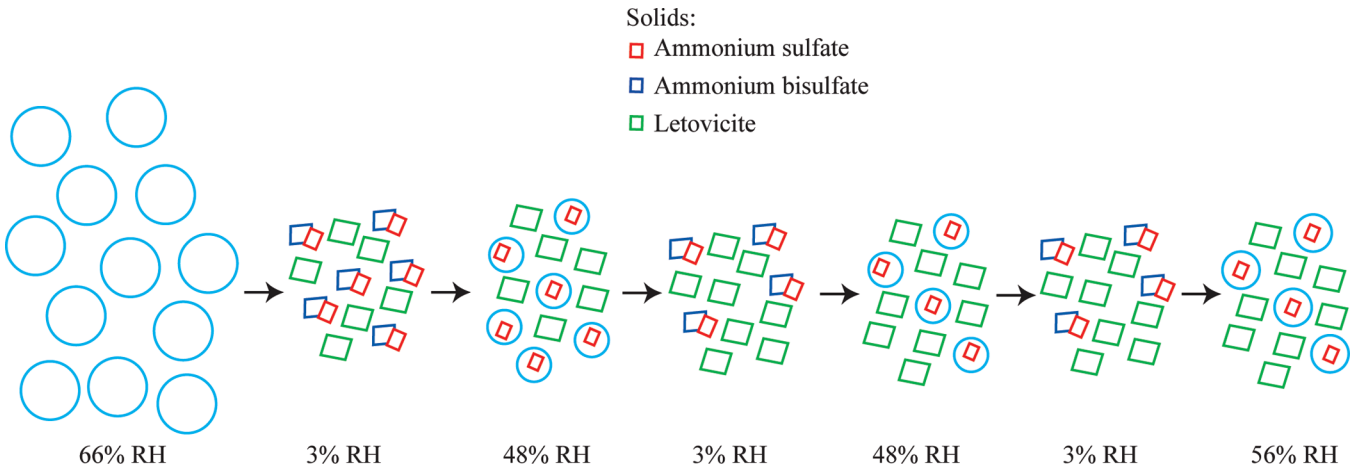

Figure 4. Cartoon illustrating the proposed mechanism for the progressive enrichment of LET particles in the externally mixed aerosol and the corresponding depletion of mixed AHS/AS particles during RH cycles between 3% and 48% for the composition [0.75, 1]. For reference, the initial deliquescence of internally mixed AHS/AS particles is expected at 27% RH and the final deliquescence is expected at 72% RH.[27] At 48% RH, ammonium sulfate cores are expected to be in equilibrium with an acidic aqueous phase. In the proposed mechanism for structural transformation, when RH drops to 3%, some of these particles nucleate letovicite, and the number concentration of letovicite particles increases. When RH is cycled back to 48%, the liquid water content is therefore reduced because there are fewer AHS/AS particles.

then be expected to be polycrystalline, rather than monocrystalline, for a strong nanosize effect to be operative, perhaps suggesting the LET crystallites are embedded within the AHS matrix prior to water uptake. Under this explanation, an additional nanosize effect that might be expected is a shift in the eutonic RH, but such a shift is not observed, at least within the RH resolution of our experiment. Biskos et al.[35] reported the absence of a nanosize effect on the deliquescence relative humidity of $(NH_4)_2SO_4$ but the presence of such an effect on its hygroscopic growth factor. The explanation is that the former is driven by differences in volume and surface tensions of aqueous/vapor and solid/vapor systems whereas the latter is driven only by the Kelvin effect and hence the aqueous/vapor surface tension.

The composition [0.70, 1] has similarities to the behavior of the more acidic particles, with two critical differences. First, the RH of initial water uptake shifts upward to between 41 and 45% RH. Second, the infrared spectrum shows the continued presence of AS. Compared to [0.75, 1], the difference spectrum (not shown) indicates that AHS/LET are enriched and AS is depleted. Although the RH of initial uptake does not appear to fit the AIM model, the detailed behavior of AHS must be considered. There is a peritonic transition (defined as solid #1 + vapor transforms into solid #2 + aqueous solution + vapor) of AHS to LET at 37% RH, but if this transition does not occur, then AHS deliquesces at 42%. The observed point of water uptake can be explained if AHS is an outer coating over cores of LET and AS. For this nanomorphology, AHS as a thin layer does not nucleate at the peritonic transition to LET but rather only deliquesces completely at 42%. This behavior can be simulated only indirectly by AIM, as done in the discussion herein, because mass is effectively temporarily removed from the thermodynamic calculation by the compartmentalization of LET and/or AS in the interior of the particle. Likewise to the more acidic compositions, after this initial water uptake no further hysteresis is observed at higher RH values for [0.70, 1], which is again a greater solubility of the solids than anticipated by AIM and possibly indicative of a nanocrystalline mixed interior. The complete solubility with abrupt water uptake above 41% RH prevented similar RH cycling experiments as done for [0.75, 1] to test for similar changes in the LET and AS/AHS balance (i.e., as attributed above to heterogeneous nucleation). Moreover, compared to [0.60, 1] and [0.65, 1], the AHS outer coating is hypothesized only for [0.70, 1], indicating the importance of drying and composition on particle morphology.

As seen in Figure 5, among the compositions studied, [0.75, 1] is unique in the comparison to the results of the AIM predictions. Specifically, a deliquescence transition at low RH is less obvious, the magnitude of the water uptake along the lower side of the hysteresis loop does not clearly follow any of the 8 cases, and the hysteresis effect is present, ruling out complete dissolution of particles at medium RH. The cartoon representation of Figure 4 does, however, rationalize the observations. Compared to the other three compositions, only [0.75, 1] nucleates some unmixed particles of pure LET. Nanocrystalline materials of pure substances can readily reconstruct to single crystals when exposed to elevated RH. Single crystalline LET crystals can account for the absence of complete dissolution at medium RH, in contrast to the behavior of the mixed crystal system for the more acidic compositions.

The magnitude of water uptake for [0.75, 1] depends on the RH cycling. The black squares in Figure 5 represent the final behavior after repeated RH cycling, representing an externally mixed population of AS/AHS and LET particles. The overall normalized water uptake is a weighted mixing of LET particles that do not take up water until higher RH (case 5 of AIM) and AS/AHS expected to take up water at 27% RH (case 4 of AIM). The observed water uptake is then a mix of cases 4 and 5, favoring more and less water uptake, respectively. Earlier in the RH cycling (e.g., the blue points), the mixing rule favors case 4 because the relative population of AS/AHS particles is higher.

At low RH, AS/AHS is expected to regulate initial water uptake for [0.75, 1], in contrast to LET/AHS for the more acidic compositions. The water peak in Figure 3 for [0.75, 1] suggests that there may be water uptake by AS/AHS at 29% that is just on the margin of detectability. In comparison, water uptake is observed only at higher RH values (cf. Figure 3) for the more acidic compositions taking up water by deliquescence of AHS for [0.70, 1] or eutonic water uptake by AHS/LET for [0.60, 1] and [0.65, 1]. The lower RH value of initial water uptake for [0.75, 1] also indicates that the magnitude of the initial water uptake will be smaller and therefore less apparent in the infrared spectra.

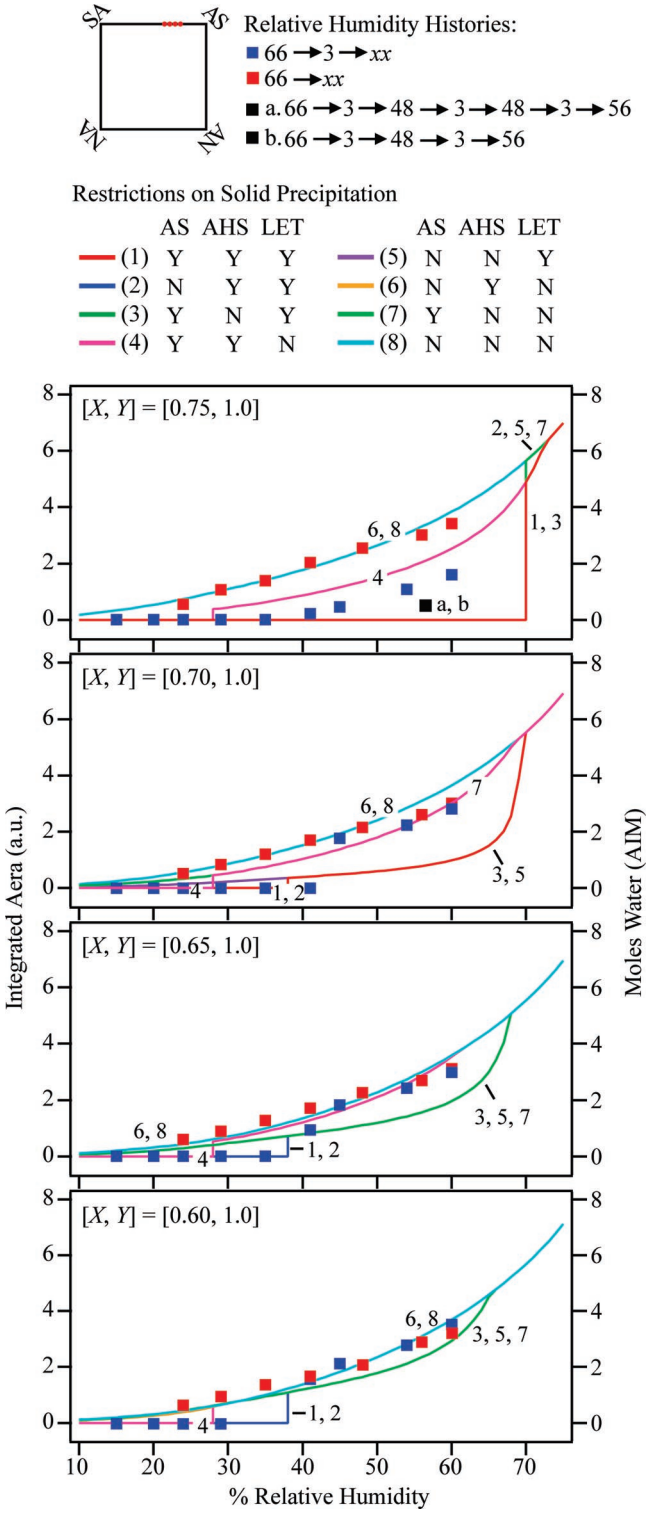

Figure 5. Comparisons of the integrated intensity of the liquid water peak (data points; left-hand axis) to the moles of water predicted by the Aerosol Inorganics Model (lines; right-hand axis).[27] For the model, eight cases that correspond to the possible permutations of solids present or absent are considered. The blue and red squares correspond to RH histories of 60 → 3 → *xx* and 60 → *xx*, respectively. Black squares *a* and *b* show the results of repeated RH cycling for the composition of [0.75, 1].

Our results for the crystals formed and subsequent water uptake by submicron particles of [0.75, 1] can be compared to results obtained for supermicron particles by Spann and Richardson[28] and Colberg et al.[14] The larger particles of those studies crystallized completely and formed letovicite between 30 and 35%, in contrast to our observations that an externally mixed population of AS/AHS and LET particles forms. Colberg et al.,[14] however, did see a range of complex crystallization pathways and morphologies for supermicron particles of [0.5, 1] composition at 260 K, although our studies at 293 K showed that submicron particles of this composition do not crystallize even to 1% RH.[9,12]

There are at least two possible explanations for the differences at [0.75, 1] between our results and those of Spann and Richardson[28] and Colberg et al.[14] Within the larger volume of supermicron particles, every particle may form one or more nuclei of LET along with AS. During crystal growth, the AS dissolves by Ostwald's ripening and LET forms completely. In comparison, when this volume is divided across submicron particles, some individual particles may form AS but not LET nuclei. The volume ratio of the particles Spann and Richardson[28] and Colberg et al.[14] to those of our study ranges from 300 to 8 $\times$ 10^6 for particle-size ranges of 2−20 μm in the earlier work and 100−300 nm in our work. A second explanation for the differences could be drying rates. Spann and Richardson[28] and Colberg et al.[14] employed approximately −1% RH per 200 s and −1% RH per 560 s, respectively. In comparison, we used a plenum with fixed low RH at the bottom so that drying rates were nonuniform. Overall, there was a 62% drop in RH (66 → 3) within 210 s, meaning that our drying rates greatly exceeded those of the cited studies. The combination of faster drying and smaller particles implies that the aqueous phase obtained higher supersaturations than in the earlier studies, possibly allowing AS to crystallize favorably to LET. For further comparison, a 1 km mixed layer at the Earth's surface cycles between low and high RH approximately every 15 min, corresponding to a 70% RH drop in 900 s based on the assumption of 30% RH at the Earth's surface. A final difference between Colberg et al.[14] and our study is temperature, which was 263.5 K in that study. Temperature can influence supersaturation, nucleation, and crystal growth rates. The differences between our observations and those of Spann and Richardson[28] and Colberg et al.[14] emphasize the need to study particle sizes and drying rates similar to those of atmospheric conditions when carrying out research on particle phase transitions and morphologies.

4. Conclusions

The results of this work suggest that multiple cycles of relative humidity could be an atmospheric process affecting the physical state of ambient particles and hence their hygroscopic growth at intermediate relative humidity. Cycling between low and medium RH can increase the fraction of more thermodynamically stable particles within an externally mixed aerosol and thus reduce water uptake. The crystal transformations are facilitated by surface-adsorbed water. For example, our experiments show that aqueous $(NH_4)_3H(SO_4)_2$ particles (X = 0.75) can crystallize to form internally mixed $(NH_4)_2SO_4$(s)/NH_4HSO_4(s) particles that convert to $(NH_4)_3H(SO_4)_2$(s) for RH cycling between 3% and 48%. The increase in the deliquescence relative humidity because of more stable crystals theoretically decreases water uptake at intermediate RH values. Chan et al.[36] similarly observed changes in the hygroscopic behavior of ammonium sulfate particles coated by glutaric acid in response to cycles of relative humidity.

There are important implications of these results regarding phase transitions both in the atmosphere and in the laboratory, along with their representation within regional and global models. In atmospheric applications, the hysteresis effect of particle phase on hygroscopic water uptake can be framed within

a back-trajectory lagrangian approach.[37] One might think to track two variables, including (1) a binary flag of whether RH last exceeded the deliquescence relative humidity or instead fell below the crystallization relative humidity and (2) the ambient RH. Our results, however, suggest that for some compositions (such as aqueous $(NH_4)_3H(SO_4)_2$ particles) additional variables of the RH history are required to accurately predict the effects of hysteresis on hygroscopic water uptake. The need to consider additional variables equally holds for laboratory experiments, such as done herein for the infrared approach but also for other common techniques such as the hygroscopic tandem differential mobility analyzer.

The specific results of this study, showing that certain compositions such as aqueous $(NH_4)_3H(SO_4)_2$ particles can form two particle populations that convert from the less to the more thermodynamically stable one with RH processing, can be generalized to some extent. External mixtures of two particle populations can occur for compositions that become highly supersaturated with respect to two solids during crystallization. The results herein show that this condition is met strongly for $X = 0.75$ and somewhat for $X = 0.70$, both of which readily nucleate LET and AS. The initial crystal is then followed by the precipitation of a second crystal such as AHS in the proportions necessary for mass balance. More acidic ($X = 0.65$) and more basic ($X = 0.80$)[12] compositions appear to nucleate only one phase. Although compositions such as $X = 0.80$ may have competitive nucleation of LET (followed by AS) or AS (followed by LET), the subpopulations would be chemically identical and therefore likely indistinguishable by our infrared technique, though subpopulations of different nanomorpholo gies might be distinguished by other techniques such as single-particle laser ablation.[38] Looking to other compositions, we previously reported[12] that an externally mixed particle population can form in the crystallization of aqueous mixtures of $(NH_4)_2SO_4$ ($Y = 1$) and NH_4NO_3 ($Y = 0$). The external population was observed at $Y = 0.4$, suggesting that $3NH_4NO_3 \cdot (NH_4)_2SO_4$(s) nucleated first in some particles and $2NH_4NO_3 \cdot (NH_4)_2SO_4$(s) in other particles, followed in both cases by the follow-on crystallization of $(NH_4)_2SO_4$(s). For $Y = 0.35$ and 0.45, a uniform particle population was observed. Although experiments were not carried out to test for the transformation of the particles of $Y = 0.35$ with RH cycling, the results of the present study lead to the hypothesis that similar behavior would be observed. In agreement with this suggestion, using an electrodynamic balance Ling and Chan[39] studied the crystallization of aqueous droplets of $Y = 0.5$ and found that metastable $3NH_4NO_3 \cdot (NH_4)_2SO_4$(s) formed and then gradually transformed into stable $2NH_4NO_3 \cdot (NH_4)_2SO_4$(s). The rate of the transformation increased with increasing relative humidity. Externally mixed particle populations were also observed by us[12] for crystallization of mixed sulfate, ammonium, nitrate, and proton solutions along the line connecting the compositions [0.7, 0.6] and [0.9, 0.2]. Externally mixed particle populations therefore may have wide applicability in more chemically complex systems, such as those occurring in the atmosphere. RH cycling could then affect the crystals present and hence the hygroscopic water uptake at medium RH values.

The results of this study also have implications for the treatment of the hysteresis effect within chemical transport models (CTM).[3,40−44] These models often omit hysteresis by making assumptions, such as that particles remain only on the upper side of the hysteresis loop (i.e., omitting all solids) or that particles follow the thermodynamic description of the lower side of the hysteresis loop (i.e., assuming crystallization and deliquescence are facile). Another heuristic employed in CTMs is that particles follow the upper side of the hysteresis loop above the crystallization relative humidity and the lower side below it. This last approach is not consistent with the requirement of a negative Gibbs free energy of a spontaneous process because a particle that has crystallized should not return to the upper side of the hysteresis loop until passing a final deliquescence relative humidity. Our results, however, show that some particles actually do dissolve in entirety just after initial deliquescence, which we suggest is because of a nanocrystalline morphology that increases the free energy of the solid phase. Morphology depends on drying rate so that, if this explanation of nanocrystalline materials is accurate, hygroscopic behavior of atmospheric particles would also depend on drying rates. Although the heuristic approach as presently applied in the literature is restricted to pure ammonium sulfate particles (which in fact once dried at 35% do not again deliquesce until 80% RH), our laboratory results do provide some support for the general assumption of a return to the upper side of the hysteresis loop beyond an initial deliquescent relative humidity for some mixed particle compositions that might have nanocrystalline morphologies.

Acknowledgment. This material is based upon work supported by the National Science Foundation under Grant No. ATM-0317583 and ATM-0633840. Any opinions, findings, and conclusions or recommendations expressed in this material are those of the authors and do not necessarily reflect the views of the National Science Foundation. T.R. received support from the Danish Agency for Science Technology and Innovation.

References and Notes

(1) Seinfeld, J. H.; Pandis, S. N. *Atmospheric Chemistry and Physics*; Wiley: New York, 1998.
(2) Penner, J. E.; Andreae, M.; Annegarn, H.; Barrie, L.; Feichter, J.; Hegg, D.; Jayaraman, A.; Leaitch, R.; Murphy, D.; Nganga, J.; Pitari, G. Aerosols, their Direct and Indirect Effects. In *In Climate Change 2001: The Scientific Basis. Contribution of Working Group I to the Third Assessment Report of the Intergovernmental Panel on Climate Change*; Houghton, J. T., Ding, Y., Griggs, D. J., Noguer, M., Linden, P. J., Dai, X., Maskell, K., Johnson, C. A., Eds.; Cambridge University Press: Cambridge, U.K., 2001; pp 289.
(3) Martin, S. T.; Hung, H. M.; Park, R. J.; Jacob, D. J.; Spurr, R. J. D.; Chance, K. V.; Chin, M. *Atmos. Chem. Phys.* **2004**, *4*, 183.
(4) Martin, S. T. *Chem. Rev.* **2000**, *100*, 3403.
(5) Hegg, D.; Larson, T.; Yuen, P. F. *J. Geophys. Res.* **1993**, *98*, 18435.
(6) Evans, M. J.; Jacob, D. J. *Geophys. Res. Lett.* **2005**, *32*, L09813.
(7) Liao, H.; Seinfeld, J. H. *J. Geophys. Res.* **2005**, *110*, D18208.
(8) Thornton, J. A.; Braban, C. F.; Abbatt, J. P. D. *Phys. Chem. Chem. Phys.* **2003**, *5*, 4593.
(9) Schlenker, J. C.; Malinowski, A.; Hung, H. M.; Rudich, Y.; Martin, S. T. *J. Phys. Chem. A* **2004**, *108*, 9375.
(10) Luna, M.; Rieutord, F.; Melman, N. A.; Dai, Q.; Salmeron, M. *J. Phys. Chem. A* **1998**, *102*, 6793.
(11) Kendall, T. A.; Martin, S. T. *Geochim. Cosmochim. Acta* **2005**, *69*, 3257.
(12) Schlenker, J. C.; Martin, S. T. *J. Phys. Chem. A* **2005**, *109*, 9980.
(13) Weis, D. D.; Ewing, G. E. *J. Geophys. Res.* **1999**, *104*, 21275.
(14) Colberg, C. A.; Krieger, U. K.; Peter, T. *J. Phys. Chem. A* **2004**, *108*, 2700.
(15) Choi, M. Y.; Chan, C. K. *Environ. Sci. Technol.* **2002**, *36*, 2422.
(16) Brooks, S. D.; Garland, R. M.; Wise, M. E.; Prenni, A. J.; Cushing, M.; Hewitt, E.; Tolbert, M. A. *J. Geophys. Res.* **2003**, *108*, 4487.
(17) Parsons, M. T.; Knopf, D. A.; Bertram, A. K. *J. Phys. Chem. A* **2004**, *108*, 11600.
(18) Braban, C. F.; Abbatt, J. P. D. *Atmos. Chem. Phys.* **2004**, *4*, 1451.
(19) Garland, R. M.; Wise, M. E.; Beaver, M. R.; DeWitt, H. L.; Aiken, A. C.; Jimenez, J. L.; Tolbert, M. A. *Atmos. Chem. Phys.* **2005**, *5*, 1951.
(20) Chan, M. N.; Lee, A. K. Y.; Chan, C. K. *Environ. Sci. Technol.* **2006**, *40*, 6983.
(21) Parsons, M. T.; Riffell, J. L.; Bertram, A. K. *J. Phys. Chem. A* **2006**, *110*, 8108.
(22) Badger, C. L.; George, I.; Griffiths, P. T.; Braban, C. F.; Cox, R. A.; Abbatt, J. P. D. *Atmos. Chem. Phys.* **2006**, *6*, 755.

(23) Takahama, S.; Pathak, R. K.; Pandis, S. N. *Environ. Sci. Technol.* **2007**, *41*, 2289.
(24) Han, J. H.; Martin, S. T. *J. Geophys. Res.* **1999**, *104*, 3543.
(25) Martin, S. T.; Han, J. H.; Hung, H. M. *Geophys. Res. Lett.* **2001**, *28*, 2601.
(26) Pant, A.; Parsons, M. T.; Bertram, A. K. *J. Phys. Chem. A* **2006**, *110*, 8701.
(27) Clegg, S. L.; Brimblecombe, P.; Wexler, A. S. *J. Phys. Chem. A* **1998**, *102*, 2137.
(28) Spann, J. F.; Richardson, C. B. *Atmos. Environ.* **1985**, *19*, 819.
(29) Tang, I. N.; Munkelwitz, H. R. *J. Geophys. Res.* **1994**, *99*, 18801.
(30) Martin, S. T.; Schlenker, J. C.; Malinowski, A.; Hung, H. M.; Rudich, Y. *Geophys. Res. Lett.* **2003**, *30*, 2102.
(31) Zuberi, B.; Bertram, A. K.; Koop, T.; Molina, L. T.; Molina, M. J. *J. Phys. Chem. A* **2001**, *105*, 6458.
(32) Fletcher, N. H. *J. Atmos. Sci.* **1969**, *26*, 1266.
(33) Gorbunov, B. Z.; Kakutkina, N. A. *J. Aerosol. Sci.* **1982**, *13*, 21.
(34) Zhang, R. Y.; Leu, M. T.; Molina, M. J. *Geophys. Res. Lett.* **1996**, *23*, 1669.
(35) Biskos, G.; Russell, L. M.; Buseck, P. R.; Martin, S. T. *Geophys. Res. Lett.* **2006**, *33*, L07801.
(36) Chan, M. N.; Lee, A. K. Y.; Chan, C. K. *Environ. Sci. Technol.* **2006**, *40*, 6983.
(37) Colberg, C. A.; Luo, B. P.; Wernli, H.; Koop, T.; Peter, T. *Atmos. Chem. Phys.* **2003**, *3*, 909.
(38) Ge, Z. Z.; Wexler, A. S.; Johnston, M. V. *J. Colloid Interface Sci.* **1996**, *183*, 68.
(39) Ling, T. Y.; Chan, C. K. *Environ. Sci. Technol.* **2007**, *41*, 8077.
(40) Boucher, O.; Anderson, T. L. *J. Geophys. Res.* **1995**, *100*, 26117.
(41) Haywood, J. M.; Roberts, D. L.; Slingo, A.; Edwards, J. M.; Shine, K. P. *J. Clim.* **1997**, *10*, 1562.
(42) Adams, P. J.; Seinfeld, J. H.; Koch, D. M. *J. Geophys. Res.* **1999**, *104*, 13791.
(43) Zhang, Y.; Seigneur, C.; Seinfeld, J. H.; Jacobson, M.; Clegg, S. L.; Binkowski, F. S. *Atmos. Environ.* **2000**, *34*, 117.
(44) Wang, J.; Hoffmann, A. H.; Park, R.; Jacob, D. J.; Martin, S. T. Submitted for publication.